International Research Journal of Engineering and Technology (IRJET) e-ISSN: 2395-0056
Volume: 07 Issue: 08 | Aug 2020 www.irjet.net p-ISSN: 2395-0072

Design and Modeling of Step-up Resonant Converter for Grid Connected HVDC System

M. Sandeep[1], M. Santosh kumar[2]

[1]M.Sandeep, M-tech Student Scholar, Dept. of Electrical & Electronics Engineering, Vikas College of Engineering and Technology, Nunna, Krishna(Dt), A.P, India.
[2]Sri.M.Santosh Kumar, Assistant Professor, Dept. of Electrical & Electronics Engineering, Vikas college of Engineering and Technology, Nunna, Krishna(Dt), A.P, India.

Abstract - *Abstract-This paper addresses the design of closed loop control of the step-up resonant converter for grid connected HVDC system based on specific criteria given. The closed loop step-up resonant converter is used to convert a low level DC input voltage from a DC power supply and use to control the average model. The average model is useful when investigating the dynamic behavior of the converter when it is subject to changes in operating parameters. The Performance analysis, which covers the closed loop control of the average model on related waveforms of output voltage discussed and achieved. The hybrid grid consists of both ac and dc networks connected together by multi directional converters. In this micro grid network, it is especially difficult to support the critical load without incessant power supply. The generated power can be extracted under varying wind speed, solar irradiation level and can be stored in batteries at low power demands. The power flow control of these devices serves to increase the system's stability. The system is simulated in Matlab/Simulink.*

Key Words: *Renewable energy, resonant converter, soft switching, voltage step-up, voltage stress.*

1. INTRODUCTION

Secondary batteries are widely used in the application of residential, industrial, and commercial energy storage systems to store electricity and supply the load for various types of electronic equipment [1]. If the dc source is directly connected to the secondary battery, the output voltage of the dc source is fixed to the voltage of the secondary battery; therefore, the system cannot always operate at each optimum operating point.

Therefore, it is necessary to install a dc–dc interface between the dc source and the secondary battery to make the energy storage system always operates at the optimum operating points. This dc–dc interface is also called the battery charger. The traditional battery charger, which extracts power from an ac-line source, requires a thyristor ac/dc converter rectifier with an equivalent series resistance to control the power flow to charge the battery system. Such a charging circuit necessarily draws a high-ripple charging current [2]. Accordingly, as the concern about the quality of a charger grows, a charging circuit for reducing the ripple and extending the battery life becomes more important in designing the battery storage systems. Several charging circuits have been proposed to overcome the disadvantages of the traditional battery charger. Unlike linear regulators, switching regulators use active power switches to operate in either the saturation region or the cutoff region [3]. Because either region will lead to low switching voltage or low switching current, it is possible to convert a dc voltage to a different level with greater efficiency, as well as with low cost, relatively small size, and light weight between the two columns. The life and capacity of the secondary batteries depend on several factors e.g., charge mode, maintenance, temperature and age. Among these factors, the charge mode has a great impact on battery life and capacity [4]. The secondary batteries should be charged with current and voltage levels with low ripple. Therefore, a high-performance battery charger is necessary in a battery energy storage system. In addition, the basic requirements of battery chargers with switching regulators are small sized and high efficiency [5]. High switching frequency is necessary to achieve a small size. However, the switching loss will increase as the switching frequency is increased. This condition, in turn, decreases the efficiency of the battery chargers. To solve this problem, some kinds of soft-switching techniques need to be used to operate switching frequency [6]-[7].One simple solution to a soft- switching converter is loaded under high resonant converters. By adopting these topologies, either voltage or current is zero during switching transition, which largely reduce the switching loss and also increase the reliability for the battery chargers. To minimize the power losses, it is essential not to waste energy in the conversion process. In relation to the power electronics and associated control schemes, the main requirement is to guarantee that the charging system is efficient [8]. Therefore, topologies with high frequencies and soft-switching technique are used to reduce the charging current ripple and extend battery life. Among these existing soft-switching converters, Resonant converters are the most popular ones because of their simplicity of circuit configuration, low switching losses, and high flexibility for charging current regulation [9].

Global energy consumption tends to grow continuously. To satisfy the demand for electric power against a background of the depletion of conventional, fossil resources the renewable energy sources are becoming more popular. According to the researches despite its fluctuating nature

and weather dependency the capacity of renewable resources can satisfy overall global and for energy. The designing of high gain DC/DC converters is imposed by severe demands [10-11].

Designers face contradictory constraints such as low cost and high reliability. First of all the inverters must be safe in terms of further maintenance as well as in relation to the environment.

Since the renewable sources can be utilized for many years the converter designers cope with long time reliability issues. The main problem for the operator is to maximize the energy yield and to minimize the maintenance. For these reasons the converters must be distinguished by high efficiency over wide input power and voltage range [12-13]. High voltage gain is required to produce sufficient DC bus voltage level. Additionally they should operate at wide temperature range expressing low EMC emission and be immune to environmental conditions. Such demands create severe constraints for DC/DC boost converter.

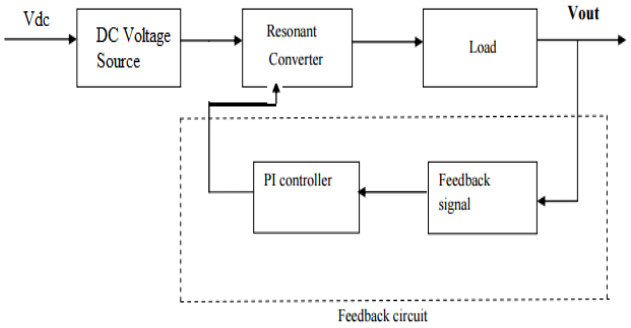

Fig.1. Block Diagram of Closed Loop Control of Step-Up Resonant Converter.

2. CONVERTER STRUCTURE AND OPERATION PRINCIPLE

The proposed resonant step-up converter is shown in Fig. 2.

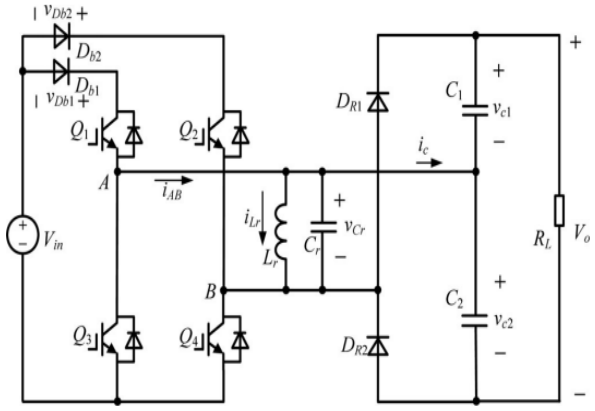

Fig. 2. Topology of the proposed resonant step-up converter.

The converter is composed of an FB switch network, which comprises Q1 through Q4, an LC parallel resonant tank, a voltage doubler rectifier, and two input blocking diodes, Db1 and Db2.

The steady-state operating waveforms are shown in Fig. 3 and detailed operation modes of the proposed converter are shown in Fig. 4. For the proposed converter, Q2 and Q3 are tuned on and off simultaneously; Q1 and Q4 are tuned on and off simultaneously. In order to simplify the analysis of the converter, the following assumptions are made:

1) All switches, diodes, inductor, and capacitor are ideal components;
2) Output filter capacitors C1 and C2 are equal and large enough so that the output voltage Vo is considered constant in a switching period Ts.

A. Mode 1 [t0, t1] [See Fig. 4(a)]

During this mode, Q1 and Q4 are turned on resulting in the positive input voltage Vin across the LC parallel resonant tank, i.e., vLr = vC r = Vin. The converter operates similar to a conventional boost converter and the resonant inductor Lr acts as the boost inductor with the current through it increasing linearly from I0. The load is powered by C1 and C2. At t1, the resonant inductor current iLr reaches I1

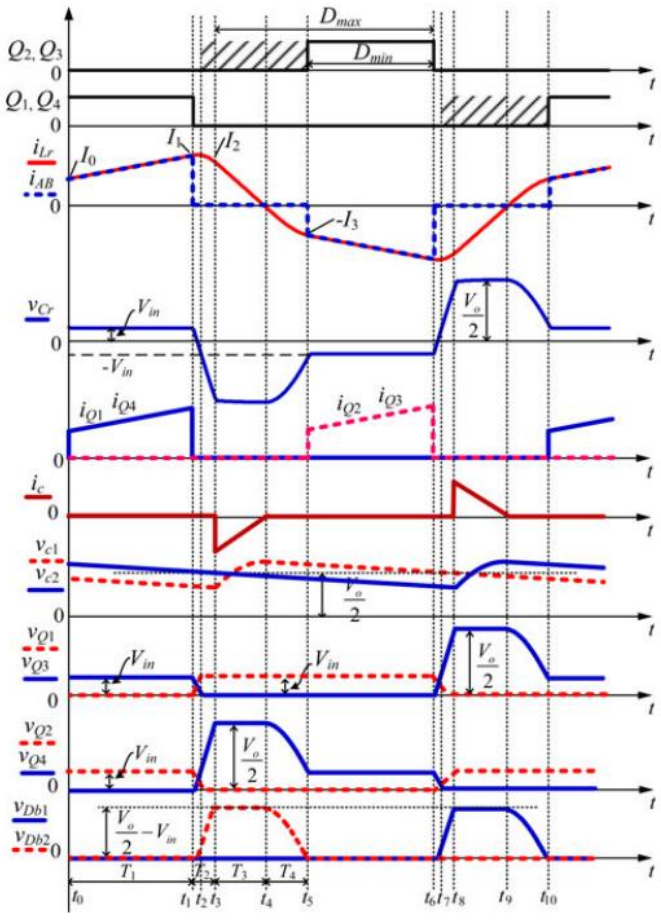

Fig. 3.Operating waveforms of the proposed converter.

$$I_1 = I_0 + \frac{V_{\text{in}} T_1}{L_r} \quad (1)$$

Where T1 is the time interval of t0 to t1.

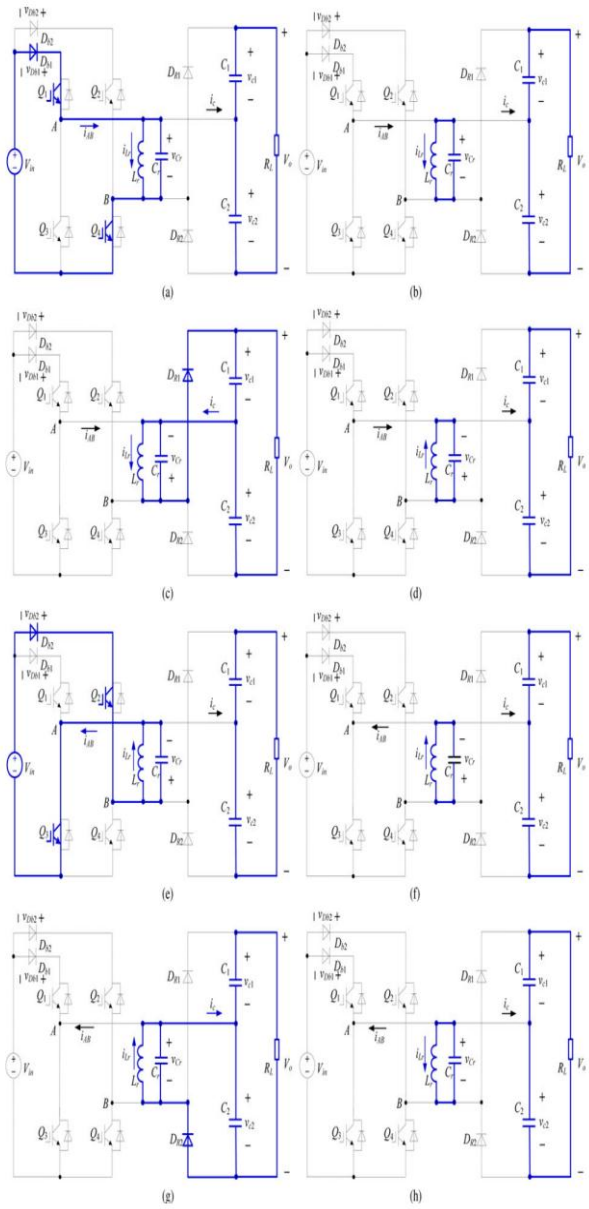

Fig. 4. Equivalent circuits of each operation stages. (a) [t0 , t1]. (b) [t1 , t3]. (c) [t3 , t4]. (d) [t4 , t5]. (e) [t5 , t6]. (f) [t6 , t8]. (g) [t8 , t9]. (h) [t9 , t10].

In this mode, the energy delivered from Vin to Lr is

$$E_{\text{in}} = \frac{1}{2} L_r (I_1^2 - I_0^2) \quad (2)$$

B. Mode 2 [t1, t3] [See Fig. 4(b)]

At t1, Q1 and Q4 are turned off and after that Lr resonates with Cr, V_{CR} decreases from Vin, and iLr increases from I1 in resonant form. Taking into account the parasitic output

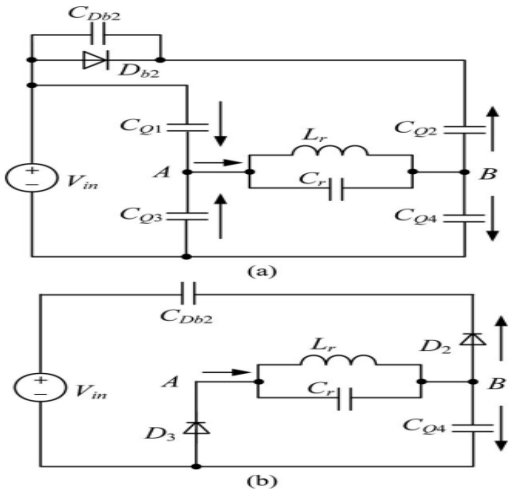

Fig. 5. Further equivalent circuits of Mode 2. (a) [t1 , t2]. (b) [t2 , t3].

Capacitors of Q1 through Q4 and junction capacitor of Db2, the equivalent circuit of the converter after t1 is shown in Fig. 5(a), in which CDb2, CQ1, and CQ4 are charged, CQ2 and CQ3 are discharged. In order to realize zero-voltage switching (ZVS) for Q2 and Q3, an additional capacitor, whose magnitude is about ten times with respect to CQ2, is connected in parallel with Db2. Hence, the voltage across Db2 is considered unchanged during the charging/discharging process and Db2 is equivalent to be shorted. Due to Cr is much larger than the parasitic capacitances, the voltages across Q1 and Q4 increase slowly. As a result, Q1 and Q4 are turned off at almost zero voltage in this mode. When V_C r drops to zero, I_{LR} reaches its maximum magnitude. After that, V_C r increases in negative direction and I_{LR} declines in resonant form. At t2, vC r = −Vin, the voltages across Q1 andQ4 reach Vin, the voltages across Q2 and Q3 fall to zero and the two switches can be turned on under zero-voltage condition. It should be noted that although Q2 and Q3 could be turned on after t2, there are no currents flowing through them. Aftert2, L_R continues to resonate with Cr, V_{CR} increases in negative direction from −Vin, I_{LR} declines in resonant form. Db2 will hold reversed-bias voltage and the voltage across Q4 continues to increase from Vin. The voltage across Q1 is kept at Vin. The equivalent circuit of the converter after t2 is shown in Fig. 5(b),in which D2 and D3 are the anti parallel diodes of Q2 and Q3,respectively. This mode runs until vC r increases to −Vo/2 and I_{LR} reduces to I2, at t3, the voltage across Q4 reaches Vo/2 and the voltage across Db2 reaches Vo/2 – Vin. It can be seen that during t1 to t3, no power is transferred from the input source or to the load, and the whole energy stored in the LC resonant tank is unchanged, i.e.,

$$\frac{1}{2} L_r I_1^2 + \frac{1}{2} C_r V_{\text{in}}^2 = \frac{1}{2} L_r I_2^2 + \frac{1}{2} C_r \left(\frac{V_o}{2}\right)^2 \quad (3)$$

We have

$$i_{Lr}(t) = \frac{V_{\text{in}}}{Z_r} \sin[\omega_r (t - t_1)] + I_1 \cos[\omega_r (t - t_1)] \quad (4)$$

$$v_{Cr}(t) = V_{\text{in}} \cos[\omega_r (t - t_1)] - I_1 Z_r \sin[\omega_r (t - t_1)] \quad (5)$$

$$T_2 = \frac{1}{\omega_r}\left[\arcsin\left(\frac{V_{\text{in}}}{\sqrt{V_{\text{in}}^2 + \frac{L_r I_1^2}{C_r}}}\right) + \arcsin\left(\frac{V_o}{2\sqrt{V_{\text{in}}^2 + \frac{L_r I_1^2}{C_r}}}\right)\right] \quad (6)$$

Where $\omega_R = 1\sqrt{LrCr}$, $Z_R = L_R/C_R$, and T2 is the time interval of t1 to t3.

C. Mode 3 [t3, t4] [See Fig.4(c)]

At t3, vC r = −Vo/2, DR1 conducts naturally, C1 is charged by iLr through DR1, V_{CR} keeps unchanged, and I_{LR} decreases linearly. At t4, I_{LR} = 0. The time interval of t3 to t4 is

$$T_3 = \frac{2I_2 L_r}{V_o} \quad (7)$$

The energy delivered to load side in this mode is

$$E_{\text{out}} = \frac{V_o I_2 T_3}{4} \quad (8)$$

The energy consumed by the load in half-switching period is

$$E_R = \frac{V_o I_o T_s}{2} \quad (9)$$

Assuming 100% conversion efficiency of the converter and according to the energy conversation rule, in half-switching period

$$E_{\text{in}} = E_{\text{out}} = E_{\text{R}} \quad (10)$$

Combining (7), (8), (9), and (10), we have

$$I_2 = V_o\sqrt{\frac{I_o T_s}{V_o L_r}} \quad (11)$$

$$T_3 = 2\sqrt{\frac{T_s I_o L_r}{V_o}} \quad (12)$$

D. Mode 4 [t4, t5] [See Fig. 4(d)]

At t4, I_{LR} decreases to zero and the current flowing throughDR1 also decreases to zero, and DR1 is turned off with zero current switching (ZCS); therefore, there is no reverse recovery. After t4, Lr resonates with Cr, Cr is discharged through L_R, V_{CR} increases from −Vo/2 in positive direction, and I_{LR} increases from zero in negative direction. Meanwhile, the voltage acrossQ4 declines from Vo/2. At t5, vC r = −Vin, and iLr = −I3. In this mode, the whole energy stored in the LC resonant tank is unchanged, i.e., where T4 is the time interval of t4 to t5.

$$\frac{1}{2}C_r\left(\frac{V_o}{2}\right)^2 = \frac{1}{2}L_r I_3^2 + \frac{1}{2}C_r V_{\text{in}}^2 \quad (13)$$

We have

$$I_0 = I_3 = \frac{1}{2}\sqrt{\frac{C_r(V_o^2 - 4V_{\text{in}}^2)}{L_r}} \quad (14)$$

$$i_{Lr}(t) = -\frac{V_o}{2\omega_r L_r}\sin\left[\omega_r(t - t_5)\right] \quad (15)$$

$$v_{Cr}(t) = \frac{-V_o\cos\left[\omega_r(t - t_5)\right]}{2} \quad (16)$$

$$T_4 = \frac{1}{\omega_r}\arccos\left(\frac{2V_{\text{in}}}{V_o}\right) \quad (17)$$

E. Mode 5 [t5, t6] [See Fig. 4(e)]

If Q2 and Q3 are turned on before t5, then after t5, L_R is charged by Vin through Q2 and Q3, I_{LR} increases in negative direction, and the mode is similar to Mode 1.If Q2 and Q3 are not turned on before t5, then after t5, L_R will resonate with Cr , the voltage of node A V_A will increase from zero and the voltage of node B V_B will decay from Vin; zero-voltage condition will be lost if Q2 and Q3 are turned on at the moment. Therefore, Q2 and Q3 must be turned on beforet5 to reduce switching loss. The operation modes during [t6, t10] are similar to Modes2–4, and the detailed equivalent circuits are shown in Fig. 4(f)–(h). During [t6, t10], Q2 and Q3 are turned off at almost zero voltage, Q1 and Q4 are turned on with ZVS, and DR2 is turned off with ZCS

3. MATLAB/SIMULATION RESULTS

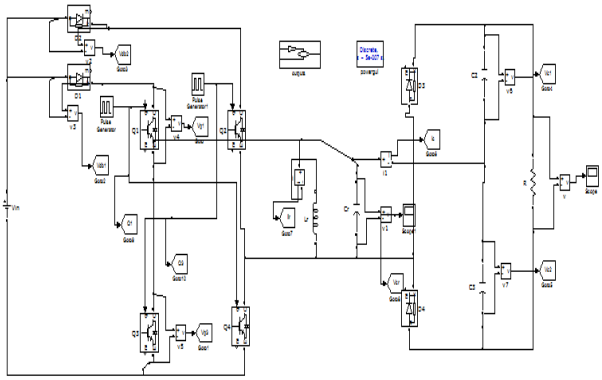

Fig.6.Simulink block diagram under 5MW load condition.

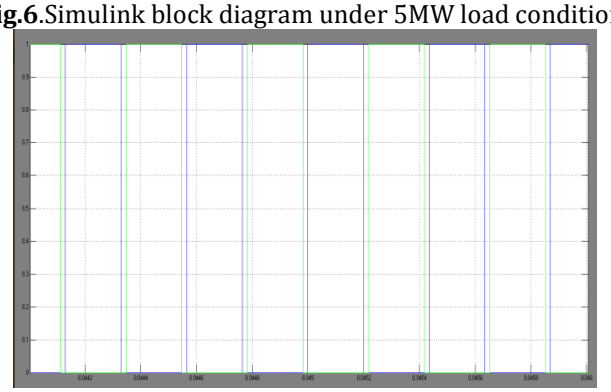

Fig.7.Simulation waveform of the switching pulses (Q1, Q2, Q3 and Q4) for 5MW.

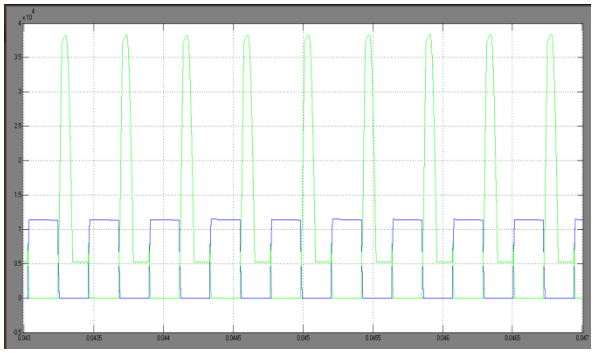

Fig.8.Simulation waveform of the switch voltages (VQ1 and VQ2) for 5MW.

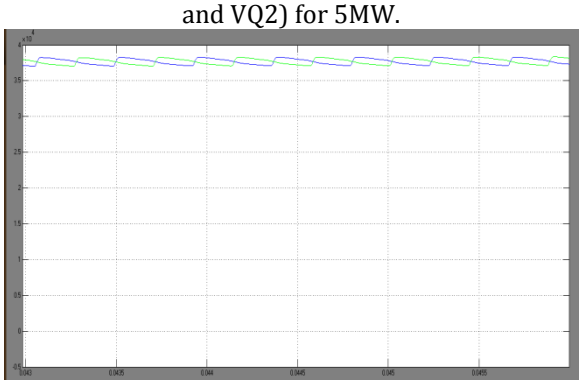

Fig.9. Simulation waveform of the output filter Capacitor Voltages (VC1 and VC2) for 5MW.

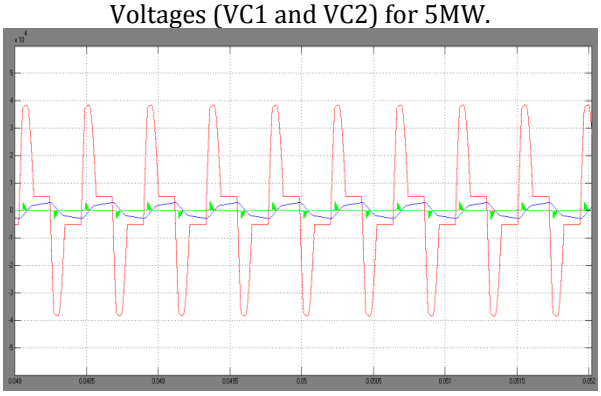

Fig.10. simulation waveform of resonant inductor current iLr, capacitor voltage and capacitor Current for 5MW.

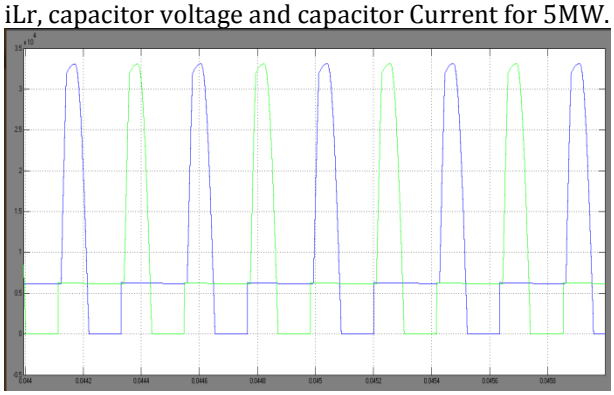

Fig.11.Simulation waveform of the input blocking diodes Voltages (VDb1 and VDb2) for 5MW.

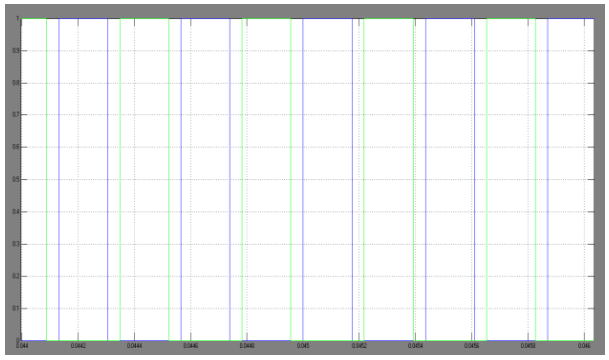

Fig.12.Simulation waveform of the switching pulses (Q1, Q2, Q3 and Q4) for 1MW.

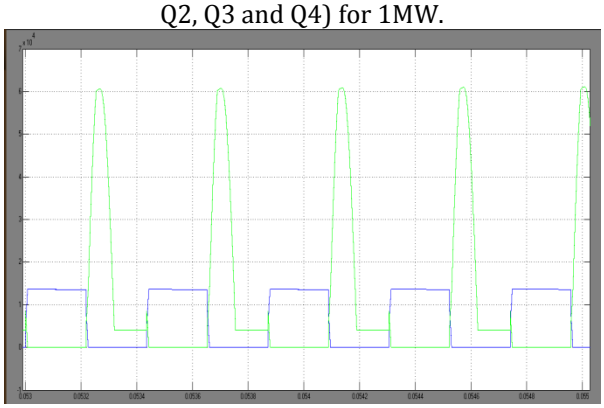

Fig.13.Simulation waveform of the switch voltages (VQ1 and VQ2) for 1MW.

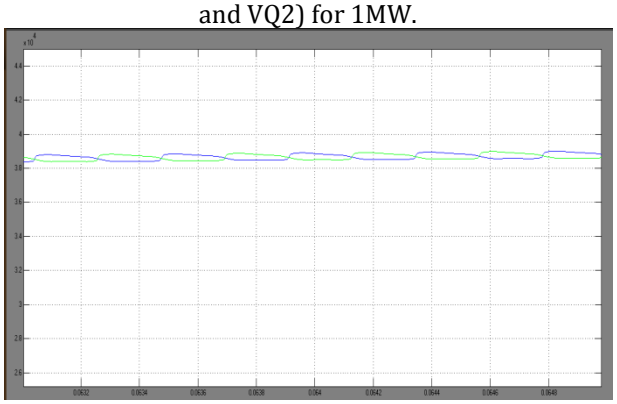

Fig.14.Simulation waveform of the output filter Capacitor Voltages (VC1 and VC2).

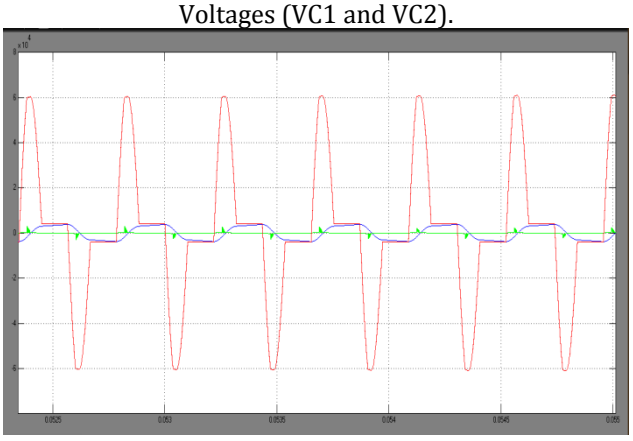

Fig.15. simulation waveform of resonant inductor current iLr, capacitor voltage and capacitor Current for 1MW.

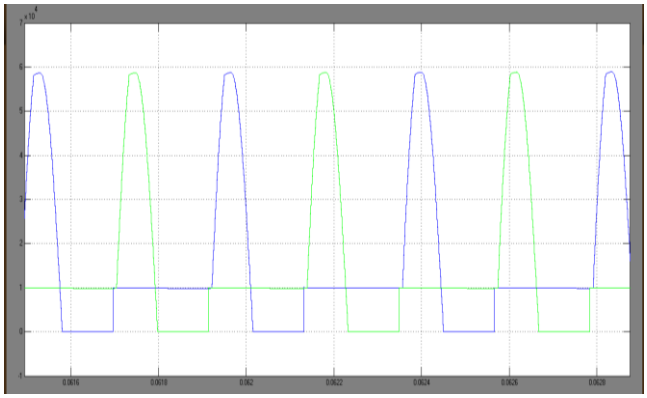

Fig.16.Simulation waveform of the input blocking diodes Voltages (VDb1 and VDb2) for 1MW.

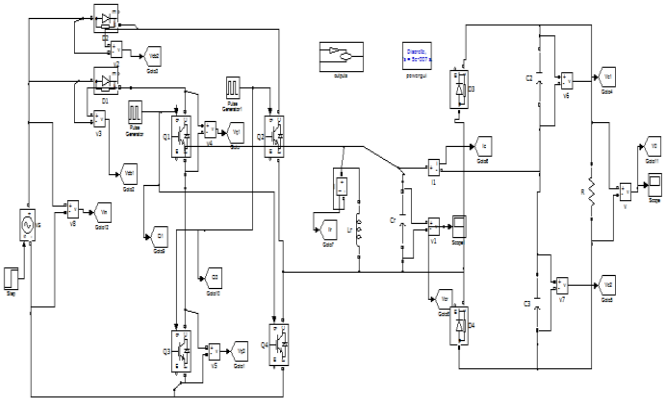

Fig.17. Simulink block diagram for input voltage step.

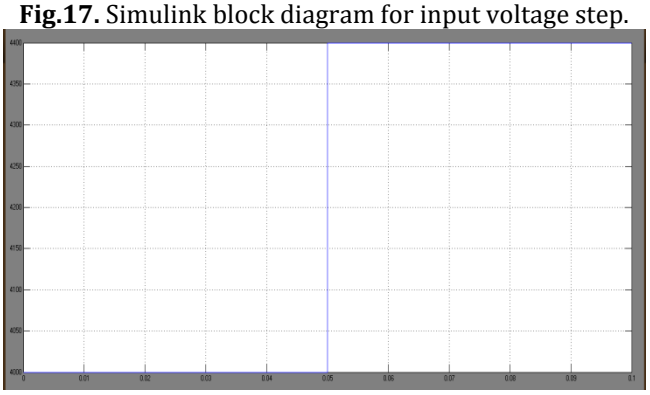

Fig.18.Input Voltage.

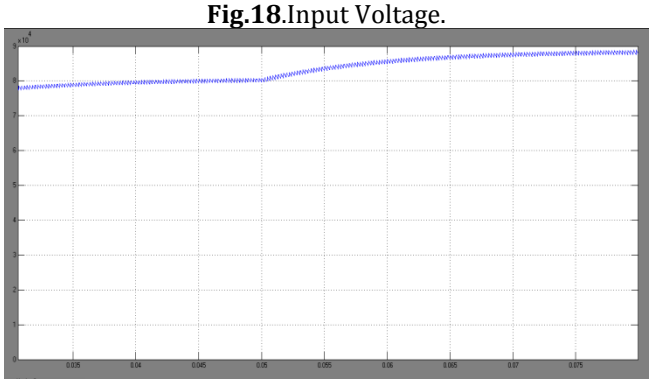

Fig.19.Output Voltage.

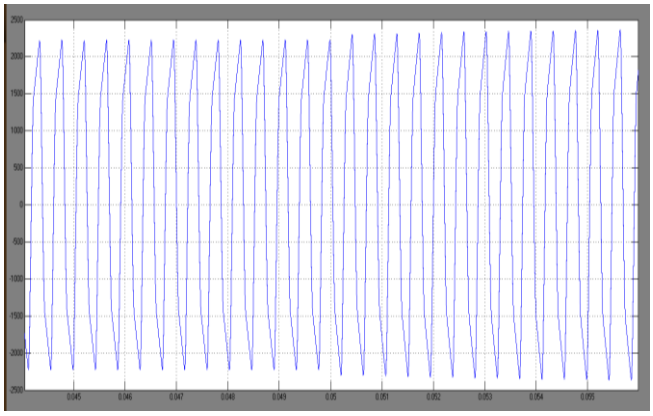

Fig.20.simulation waveform of resonant inductor current iLr.

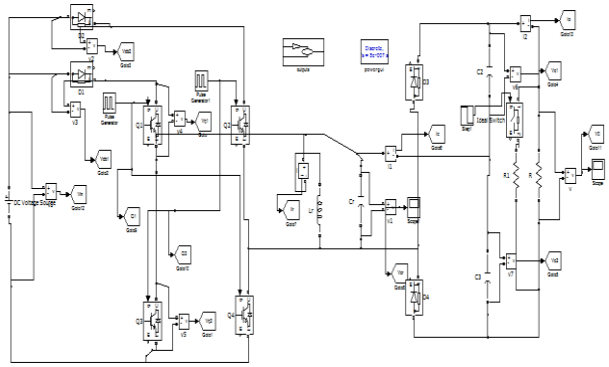

Fig.21.Simulink block diagram for step load.

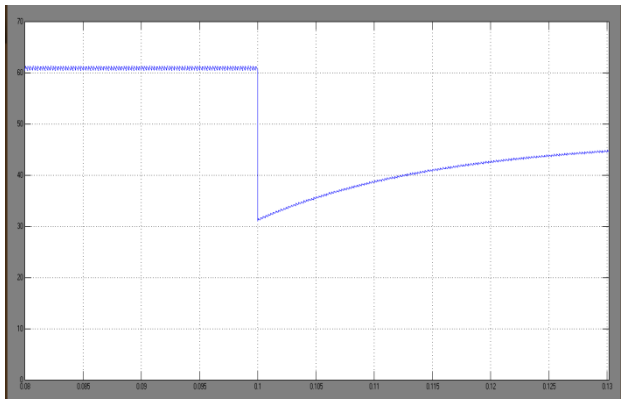

Fig.22.Input Voltage.

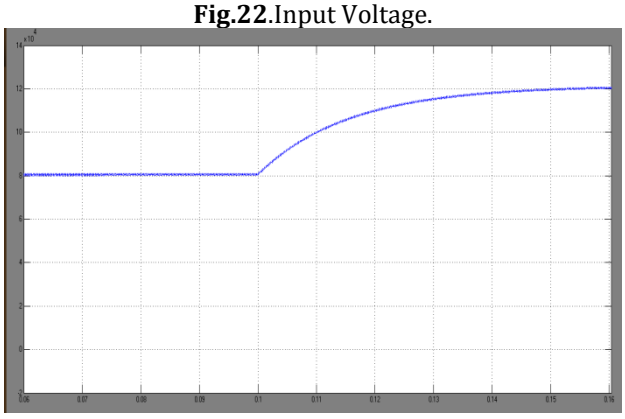

Fig.23. Output Voltage.

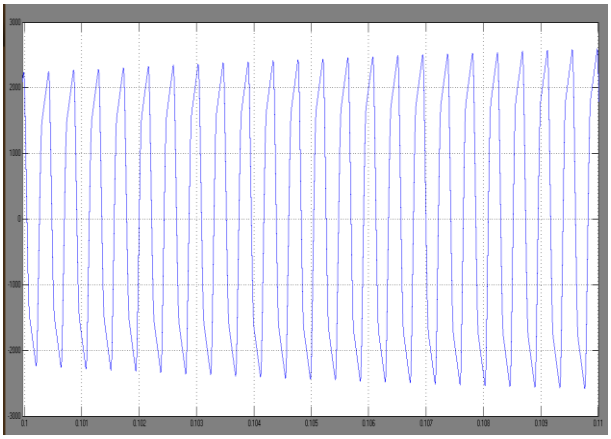

Fig.24. Simulation waveform of resonant inductor current iLr.

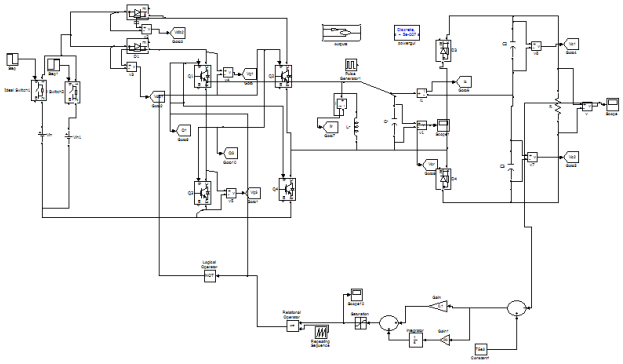

Fig.25. Simulink block diagram for input variation of Closed loop Control Step-up Resonant Converter.

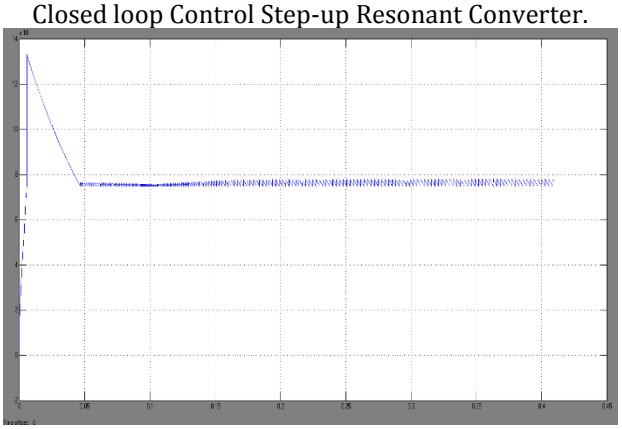

Fig.26. Simulation waveform of input variation of Closed loop Control Step-up Resonant Converter output Voltage.

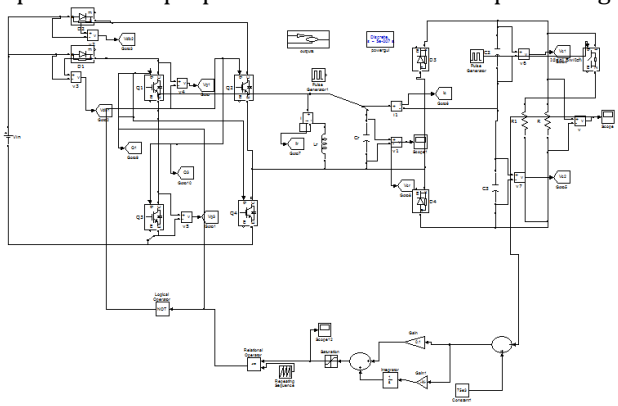

Fig.27. Simulink block diagram for Load variation of Closed loop Control Step-up Resonant Converter.

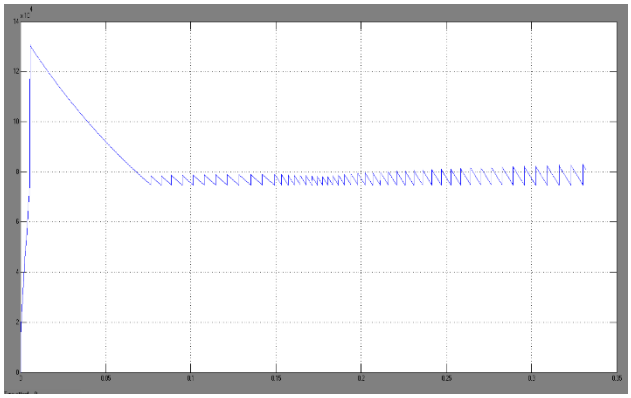

Fig.28. Simulation waveform of load variation of Closed loop Control Step-up Resonant Converter output Voltage.

CONCUSIONS

A new topology was proposed to improve the resonant converter with the following main characteristics: high boost voltage inversion ability, continuous input current, and resonance suppression at startup. For the same transformer turn ratio and input and output voltage, the improved inverter has a higher modulation index with reduced voltage stress on the dc link, lower current stress flow to the transformer windings and diode, and lower input current ripple. The converter utilizes the resonant inductor to deliver power by charging from the input and discharging at the output. The resonant capacitor is employed to achieve zero-voltage turn-on and turn-off for the active switches and ZCS for the rectifier diodes. This type of impedance network can be used for high step-up inversion ability, and continuous input current. By using compensate the amplifier makes the compensation of the boost converter much easier as the power stage has a response of the system at low frequency and using a compensator, is adequate, which greatly simplifies the design process. And the controller can stabilize the output voltage when the load is changing.

REFERENCES

[1].Wu Chen, Member, IEEE, Xiaogang Wu, Liangzhong Yao, Senior Member, IEEE, Wei Jiang, Member, IEEE, and Renjie Hu"A Step-up Resonant Converter for Grid-Connected Renewable Energy Sources"IEEE Transactions On Power Electronics, Vol. 30, No. 6, June 2015.

[2] CIGRE B4-52 Working Group, HVDC Grid Feasibility Study. Melbourne, Vic., Australia: Int. Council Large Electr. Syst., 2011.

[3] A. S. Abdel-Khalik, A. M. Massoud, A. A. Elserougi, and S. Ahmed, "Optimum power transmission-based droop control design for multi-terminal HVDC of offshore wind farms," IEEE Trans. Power Syst., vol. 28, no. 3, pp. 3401–3409, Aug. 2013.

[4] F. Deng and Z. Chen, "Design of protective inductors for HVDC transmission line within DC grid offshore wind farms," IEEE Trans. Power Del., vol. 28, no. 1, pp. 75–83, Jan. 2013.

[5] F. Deng and Z. Chen, "Operation and control of a DC-grid offshore wind farm under DC transmission system faults,"

IEEE Trans. Power Del., vol. 28, no. 1, pp. 1356–1363, Jul. 2013.
[6] C. Meyer, "Key components for future offshore DC grids," Ph.D. dissertation, RWTH Aachen Univ., Aachen, Germany, pp. 9–12, 2007.
[7] W. Chen, A. Huang, S. Lukic, J. Svensson, J. Li, and Z. Wang, "A comparison of medium voltage high power DC/DC converters with high step-up conversion ratio for offshore wind energy systems," in Proc. IEEE Energy Convers. Congr. Expo., 2011, pp. 584–589.
[8] L. Max, "Design and control of a DC collection grid for a wind farm," Ph.D. dissertation, Chalmers Univ. Technol., Goteborg, Sweden, pp. 15– ¨30, 2009.
[9] Y. Zhou, D. Macpherson, W. Blewitt, and D. Jovcic, "Comparison of DCDC converter topologies for offshore wind-farm application," in Proc. Int. Conf. Power Electron. Mach. Drives, 2012, pp. 1–6.
[10] S. Fan, W. Ma, T. C. Lim, and B. W. Williams, "Design and control of a wind energy conversion system based on a resonant dc/dc converter," IET Renew. Power Gener., vol. 7, no. 3, pp. 265–274, 2013.
[11] F. Deng and Z. Chen, "Control of improved full-bridge three-level DC/DC converter for wind turbines in a DC grid," IEEE Trans. Power Electron., vol. 28, no. 1, pp. 314–324, Jan. 2013.
[12] C. Meyer, M. Hoing, A. Peterson, and R. W. De Doncker, "Control and ¨ design of DC grids for offshore wind farms," IEEE Trans. Ind. Appl., vol. 43, no. 6, pp. 1475–1482, Nov./Dec. 2007.
[13] C. Meyer and R. W. De Doncker, "Design of a three-phase series resonant converter for offshore DC grids," in Proc. IEEE Ind. Appl. Soc. Conf., 2007, pp. 216–223.